

Spin-polarized electron scattering from pseudomorphic Au on Ir(001)J. Kirschner,¹ F. Giebels,² H. Gollisch,² and R. Feder^{1,2}¹*Max-Planck Institut für Mikrostrukturphysik, Weinberg 2, 06120 Halle, Germany*²*Theoretische Festkörperphysik, Universität Duisburg-Essen, 47048 Duisburg, Germany*

(Received 3 May 2013; revised manuscript received 15 July 2013; published 16 September 2013)

A pseudomorphic monolayer of Au on Ir(001) is easily preparable and has a long lifetime in ultrahigh vacuum. Its geometrical and electronic structure was investigated by *ab initio* calculations within density functional theory. For a wide range of energies (below 100 eV) and angles of incidence of spin-polarized primary electrons we measured and calculated the intensity and spin asymmetry of the specularly reflected beam. In the resulting energy-angular maps, which show good agreement between experiment and theory, we identify several regions of high asymmetry and sizable intensity. These regions, together with the long lifetime in ultrahigh vacuum, make pseudomorphic Au on Ir(001) very suitable as a two-dimensional spin-polarizing mirror in momentum microscopes and behind dispersive electron energy analyzers.

DOI: [10.1103/PhysRevB.88.125419](https://doi.org/10.1103/PhysRevB.88.125419)

PACS number(s): 68.49.Jk, 71.70.Ej

I. INTRODUCTION

Spin-polarized electron spectroscopy has received increasing interest in recent years because of the rich information contained in the magnitude and orientation of the spin-polarization vector, e.g., in photoemission from magnetic and nonmagnetic solids. An important class of spin-polarization analyzers is based on the elastic diffraction of electrons from single crystal surfaces of heavy materials, thus making use of the spin-orbit interaction. In practical application it is important that the surface stay clean and stable over extended periods of time and that, once it gets contaminated, there is an easy and reproducible procedure to create a fresh surface. In the following we show that a pseudomorphic monolayer of Au on Ir fulfills these requirements.

In 1949 van der Merwe and Frank pointed out,¹ based on theoretical considerations, the possibility of pseudomorphic growth of material *A* on a crystal *B*, i.e., maintaining the surface lattice of *B*, provided that the lattice mismatch was not too large ($\approx 10\%$). Apparently the first experimental observation of a clean pseudomorphic monolayer was made in Ref. 2 for Th on Ta(001) using low-energy electron diffraction (LEED), Auger spectroscopy, and a calibrated source of Th. Subsequently many other systems were found. The motivation may have been sheer scientific curiosity [e.g., “Do pseudomorphic monolayers form on nonperiodic substrates?” (the answer is “yes”; see the review article, Ref. 3)], or to use bimetallic surfaces as a model for heterogeneous catalysts. For example, it has been observed that the catalytic activity of a pseudomorphic monolayer is different from that of a clean surface of each of the constituents; see Ref. 4 and references therein. Similarly, the magnetic properties of a pseudomorphic layer may be substantially different from that of a multilayer of a ferromagnetic material. [For example the magnetic moment per atom in a pseudomorphic monolayer of Fe on W(110) is enhanced by 14% relative to its value in bulk Fe.⁵]

Our interest in pseudomorphic monolayers was motivated by our search for a stable target for a multichannel spin-polarization detector based on spin orbit coupling.^{6,7} It should provide high polarization sensitivity, long lifetime in vacuum, and should easily and reproducibly be prepared. Candidates are in principle all high-*Z* materials meeting the above

requirements. The W(001) detector⁸ has proven its merits and has been well characterized.^{9,10} However, it suffers from the sensitivity of W to reactive gases, even in ultrahigh vacuum (UHV), which limits its useful lifetime to about 1 h after a high-temperature flash. We concentrated our search for a more stable target on Ir and Au, both with a (100) surface. From a practical point of view a fourfold symmetric surface is preferable, though not mandatory, in the spin detector application for the following reason: If the scattering plane coincides with a mirror plane of the crystal then the asymmetry vector stands perpendicular to that plane.¹¹ While this can be obtained also with a two fold symmetric surface, the alignment checks are facilitated if equivalent beams can be compared.

Unfortunately, both Ir(100) and Au(100) are reconstructed in thermodynamic equilibrium. Ir shows a (5×1) reconstruction with two orthogonal domains, not necessarily in equal proportions. Au(100) has a complicated superstructure, due to a hexagonal overlayer, with a LEED pattern described as $(5 \times n)$ with *n* ranging from 26 to 28¹² [resembling superficially a (5×1) pattern]. There are ways and means to lift these reconstructions for both Ir and Au, but these procedures are at variance with our requirement of simple and easy preparation. In principle, the multichannel spin-polarized LEED (SPLEED) detector based on the specular beam works also with a reconstructed surface, provided that the specular beam is reproducible and that the higher order beams are not detected. This has been shown for the Ir(100) surface recently.¹³

The most inert metal surface in vacuum is that of Au. For the spin detector based on diffuse electron scattering from Au, Unguris *et al.*¹⁴ reported a useful lifetime of several weeks in UHV. Therefore a Au single crystal would be an excellent alternative if the reconstruction problem could be overcome. This led us to consider epitaxial Au films on Ir(100): Au for its inertness and ease of deposition and Ir for its ease of preparation, requiring little more than a high-temperature treatment. At first sight, it seems rather hopeless to obtain an unreconstructed (1×1) surface in such an epitaxial system, where both components deeply reconstruct into a similar pattern. Indeed, this system has rarely been described in the literature. An early work in 1970 by Thomas reported

a nearly ideal layer-by-layer growth of Au on Ir(111)¹⁵ at room temperature, the films being stable up to 700 °C, with thicknesses up to 8 nm, and a (111) LEED pattern. It took more than 30 years until this system received renewed interest, when Okada demonstrated that dissociative adsorption of H₂ occurs on thin Au(111) films,¹⁶ in contrast to the surface of bulk Au(111) which cannot dissociate H₂.

The paper is organized as follows. In Sec. II we summarize present knowledge about thin Au films on Ir. Section III deals with experimental aspects. In Sec. IV we report on *ab initio* theory of the film geometry and outline specific features of our SPLEED calculations. Experimental and theoretical SPLEED results are presented in Sec. V, followed by a conclusion in Sec. VI.

II. PROPERTIES OF THIN Au FILMS ON Ir

In this section we summarize the presently known facts for Au on Ir (to our knowledge), partly taken from previous experiments, from theoretical calculations, and from our own observations.

(1) Thin films of Au on Ir(111) and on Ir(100) grow in a layer-by-layer mode at 300 K. For (111) this was observed directly by scanning tunneling microscopy (STM),¹⁷ for (100) from our LEED intensity oscillations.

(2) The first layer shows dissociative adsorption of H₂, whereas bulk Au does not. This was proven by nuclear reaction analysis.^{16,18,19} The H coverage at 60 K is about 0.06 monolayers (ML), independent of H₂ exposure up to 3×10^3 L.

(3) Different theories unanimously predict strong segregation of Au to Ir surfaces,^{20–22} also for the more open (100) surface.²² The surface mixing energy is strongly negative, which means that there is no intermixing within the surface layer.²¹ This was confirmed for Ir (111) by scanning tunneling microscopy.¹⁷ Thus, there should be no intermixing of Au in Ir, fully in line with our own observations.

(4) Upon deposition of Au on Ir(100) 5×1 at 300 K we observe that the reconstruction of Ir is lifted upon deposition of about 0.2 ML of Au and that it does not reappear at higher dosage. With a few monolayers of Au the surface shows a (1×1) LEED pattern, though somewhat diffuse. Upon annealing this surface at about 700 °C a faint (5×1) structure appears, similar to but not identical to the (5×26) pattern of the bulk Au(100) surface.

(5) Starting at about 800 °C the multilayers of Au desorb until the pseudomorphic monolayer remains. About 900 °C is needed to desorb the pseudomorphic monolayer; heating to 1200 °C brings the clean Ir(100) (5×1) back, with no Au visible in the Auger spectrum.

III. EXPERIMENTAL ASPECTS

A diagram of our experimental setup is shown in Fig. 1. The experiments were carried out in a μ -metal UHV chamber equipped with a cylindrical mirror analyzer (CMA) Auger analyzer, a MEED (medium energy electron diffraction) screen opposite to the CMA, a quartz crystal monitor, and an evaporation source.²³ This scattering chamber was pumped by an ion getter pump and a turbo pump. The base pres-

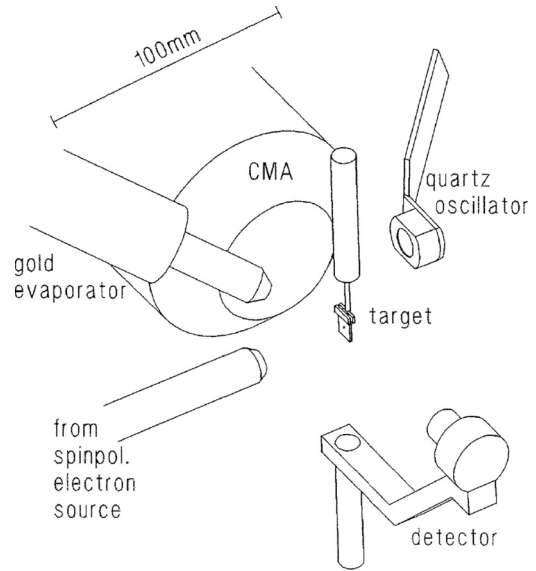


FIG. 1. Experimental setup.

sure was 7×10^{-11} mbar or less, rising to 3×10^{-10} mbar during Au evaporation. Unlike usual LEED experiments a goniometer type system was used. The Ir crystal was mounted on a vertical motor-driven rotation feed-through with optical angle encoder and heated by electron bombardment. Temperature was measured by a pyrometer and a thermocouple attached to the crystal. The repeatability of the angle setting was better than 0.1 degree. The same type of mounting was used for the electron detector. A circular case was mounted on the detector arm, moving horizontally, having an entrance aperture of 5 mm diameter, followed by a grounded mesh, an identical mesh on a retarding potential (the primary electron beam voltage minus a battery voltage of 3.1 V), then followed by a double channel-plate electron detector. The overall angular resolution (beam spread folded with the detector resolution) was measured to be about 2 degrees FWHM, with a distance of 90 mm from sample to entrance aperture.

The polarized electron source chamber is separated from the scattering chamber by a small gate valve with the electron beam passing through its center. The chamber is likewise made of μ -metal and pumped by an ion getter pump. The base pressure is 6×10^{-11} mbar. The photocathode is a strained multilayer of GaAs as described in Ref. 24. The cathode was cleaned by a beam of atomic hydrogen²⁵ at 420 °C, then heated in UHV at 420–490 °C and activated by Cs and O₂ according to the usual yo-yo procedure. The spin-polarized electrons are excited by circularly polarized 828 nm photons from a laser diode, a fiber optics and an electrooptical modulator.²⁶ The degree of circular polarization was determined by an optical polarimeter²⁷ to be 92% averaged over the two settings of the optical modulator for positive and negative helicity, disregarding a possible depolarization by the standard UHV glass window. The primary beam intensity impinging on the Ir crystal was determined by the rotatable electron detector in the forward direction after retracting the target out of the beam. The reflectivity and figure-of-merit spectra have been normalized by the primary beam intensity.

The preparation of the pseudomorphic Au monolayer on the Ir crystal was done in the following way: first removing the carbon by repeated heating cycles in O₂ according to the procedure described in Ref. 28. The residual oxygen is removed by flashing to 1200 °C, leaving a clean Ir(100) 5 × 1 surface. Next, an equivalent of 1.5 to 2 ML of Au is deposited, controlled by the quartz crystal oscillator, placed at the target position. Then the crystal is heated by multiple flashes at temperatures below the desorption temperature of the pseudomorphic Au monolayer. The process is monitored *in situ* by measuring the asymmetry in the (00) beam until a maximum raw asymmetry of 62% to 63% is reached (primary voltage 44 V, polar angle $\vartheta = 45^\circ$, azimuth $\varphi = 0^\circ$). This heating procedure is self-limiting because the desorption temperature for Au multilayers is lower by 50–80 K than that of the pseudomorphic monolayer. The measured asymmetry is extraordinarily stable at the base pressure condition quoted above. The measurements shown in this paper have intentionally been made with a pseudomorphic monolayer prepared 3 weeks prior to the measurements. No degradation of the asymmetry was found during this period. The data shown in the following have been obtained as energy spectra at constant polar angle ϑ , with an energy step width of 0.1 eV. The step width of ϑ is 1 degree. Thus the experimental maps contain more than 40 000 data points.

IV. THEORY

In this section we firstly report on *ab initio* calculations of the geometrical and electronic structure of the ground state of pseudomorphic Au films on Ir(001) and secondly address key aspects of our SPLEED calculations.

As deduced above, the Au/Ir(001) surface system in our experiment consists of a pseudomorphic monolayer of Au on an Ir(001) 1 × 1 surface. The observed 1 × 1 LEED pattern implies that the Au layer has the same unit cell as the adjacent Ir layers and the Au atoms are all within a single plane. Their surface-parallel positions are the same as those of the Ir atoms in the second Ir layer, i.e., fourfold hollow sites of the first Ir layer, which are energetically more favorable than other conceivable sites. Not yet known, however, are the spacing between the Au layer and the topmost Ir layer and the spacings between the near-surface Ir layers.

To obtain these interlayer spacings, we resorted to first-principles calculations in the framework of density functional theory. We employed the full-potential linearized augmented plane wave method²⁹ with a local density approximation for the exchange-correlation energy³⁰ as implemented in the Juelich FLEUR computer code.³¹ For a nine-layer film, which consists of seven Ir layers and an Au monolayer on each side, we allowed the topmost three interlayer spacings to relax such that the total energy became minimal and the forces on the atoms were practically zero. The results are shown in Table I.

According to Table I the spacing $d_{\text{Au-Ir}}$ between the Au and the topmost Ir layer is 2.08 Å, which is larger than the interlayer spacing in bulk Au (2.04 Å) due to the lateral compression of the Au layer. If—instead of employing sophisticated *ab initio* theory—one simply assumes the conservation of the atomic volume of the respective bulk materials, one obtains $\delta_{\text{Au-Ir}} = 10\%$ corresponding to $d_{\text{Au-Ir}} = 2.11$ Å. Compared to

TABLE I. Pseudomorphic films of 1 and 2 ML Au on Ir(001): interlayer distances from density functional calculations, represented by the differences δ (in percent) with respect to the bulk interlayer distance of Ir(001) 1.92 Å. $\delta_{\text{Ir-Ir}}^{(1)}$ ($\delta_{\text{Ir-Ir}}^{(2)}$) refers to the spacing between the first and the second (second and third) Ir layer.

| | $\delta_{\text{Au-Au}}$ | $\delta_{\text{Au-Ir}}$ | $\delta_{\text{Ir-Ir}}^{(1)}$ | $\delta_{\text{Ir-Ir}}^{(2)}$ |
|---------------|-------------------------|-------------------------|-------------------------------|-------------------------------|
| 1 ML Au on Ir | | 8.4% | −4.4% | −0.4% |
| 2 ML Au on Ir | 15.0% | 11.0% | −3.6% | 0.8% |

the latter value, the *ab initio* theory thus yields an inward relaxation of 1.4%.

Although our experimental surface system was found to consist of a pseudomorphic monolayer of Au on Ir(001), we would like to explore theoretically how the addition of a second pseudomorphic Au layer affects SPLEED intensities and asymmetries. This is of interest in its own right and useful for corroborating our experimental finding of 1 ML by comparing the experimental SPLEED data with their theoretical counterparts for 1 and 2 ML. Pseudomorphic double layers of Au were actually reported to exist on Pd(001)³² and on Pt(001),^{33,34} whereas on Rh(001), for which the lattice mismatch is larger, the second Au monolayer already exhibits a hexagonal close packed (hcp) type reconstruction similar to the one of the Au(001) surface.³⁵ For Au on Ir(001), a reconstruction appears for a coverage of a few ML (cf. item 4 of Sec. II).

In the following we assume the second Au layer to be pseudomorphic, which leaves the interlayer distances to be determined. We calculated them *ab initio* (as described above for 1 ML) using an 11-layer film, which consists of 7 Ir layers and 2 Au layers on each side. The results are shown in Table I. The corresponding absolute interlayer spacings are $d_{\text{Au-Au}} = 2.21$ Å and $d_{\text{Au-Ir}} = 2.13$ Å. For the Au-Au spacing, the above-mentioned atomic volume argument yields $\delta_{\text{Au-Au}} = 20\%$, equivalent to $d_{\text{Au-Au}} = 2.30$ Å. Compared to the latter, the *ab initio* theory thus yields an inward relaxation of 3.9%.

For the pseudomorphic 1 ML and the 2 ML systems with interlayer spacings as listed in Table I, our FLAPW calculations also yielded the electronic structure of the ground state, in particular real one-electron potentials.

To obtain the quasiparticle potentials, which were needed as input for our SPLEED calculations, the ground state real potential for each system was augmented by a complex self-energy correction. The choice of its imaginary part, which accounts for the influence of inelastic scattering, was guided by the decrease of our experimental intensities with increasing kinetic energy E . As a satisfactory form we thus found $V_i(E) = 0.42(E + 5)^{0.5}$ eV, with E in eV.

The real part of the self-energy correction has essentially two components. Firstly, the ground state real inner potential is reduced. Secondly, the surface potential barrier, which is obtained by the ground state calculation, has to be modified such that asymptotically it has the image potential form $1/z$, where z is the coordinate normal to the surface. For details of the form of our surface barrier see Ref. 36 and references therein.

Using the above quasiparticle potential, SPLEED calculations were performed by means of a relativistic layer Korringa-Kohn-Rostoker (KKR) code.¹¹ For a primary beam with intensity 1 and spin polarization $\pm 100\%$ normal to the scattering plane we thus obtained spin-dependent intensities I^+ and I^- as functions of the kinetic energy E and the polar angle of incidence ϑ . These two intensities are equivalent to the spin-averaged intensity $I = 0.5(I^+ + I^-)$ and the asymmetry $A = 100(I^+ - I^-)/(I^+ + I^-)$. The figure of merit, which characterizes the efficiency for spin detection, is then $F = I \times A^2 \times 10^{-4}$. Note that, according to the above definition, the asymmetry A ranges from -100% to $+100\%$.

V. SPLEED ENERGY-ANGULAR MAPS

In Fig. 2 we present our experimental and theoretical SPLEED specular beam results for a pseudomorphic

monolayer of Au on Ir(001) as functions of the energy and the polar angle of incidence. The scattering plane intersects the surface plane along the [100] direction (azimuthal angle $\varphi = 0^\circ$). A bird's eye inspection of the energy-angular landscapes of intensities, asymmetries, and figures of merit reveals a good overall agreement between experiment and theory. Before going into details, we would like to contrast this with the analogous theoretical landscapes for two pseudomorphic monolayers of Au on Ir(001) shown in Fig. 3. They agree visibly less with our experimental results in Fig. 2. Theoretical results for 1 ML Au/Ir(001) for azimuthal angle $\varphi = 45^\circ$, which are shown in Fig. 4, differ strongly from both theoretical and experimental results in Fig. 2.

Wishing to complement our visual evaluation by a quantitative measure of agreement, we first thought of so-called reliability factors (R factors), which were proposed for LEED intensity spectra (cf. Ref. 37 and references therein) and

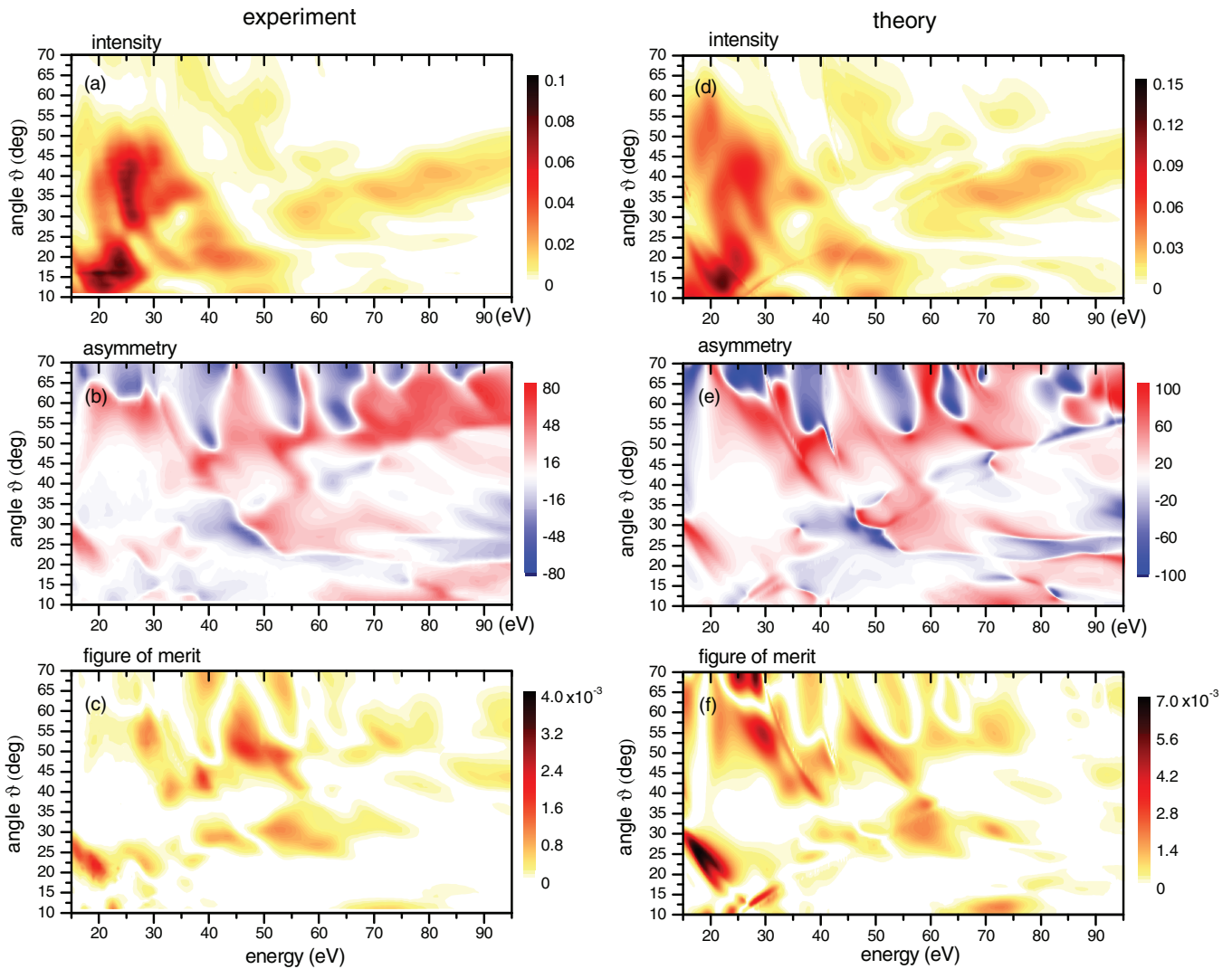


FIG. 2. (Color) Specular reflection of spin-polarized electrons from a pseudomorphic monolayer of Au on Ir(001). With coordinates x and y chosen in the surface plane along [100] and [010], respectively, and z along the surface normal [001], the primary electrons with energy E and spin orientation axis y impinge on the surface in the (x, z) plane at polar angle ϑ (relative to the surface normal) and azimuthal angle $\varphi = 0^\circ$, i.e. with surface-parallel momentum ($k_x < 0, k_y = 0$). The specular beam results are displayed as functions of the energy E and the polar angle of incidence ϑ . Left-hand panels: Experiment; intensity I , measured raw asymmetry A_{raw} (in percent), and figure of merit $IA_{\text{raw}}^2 \times 10^{-4}$. Right-hand panels: Theory; intensity I , asymmetry A (in percent), and figure of merit $IA^2 \times 10^{-4}$.

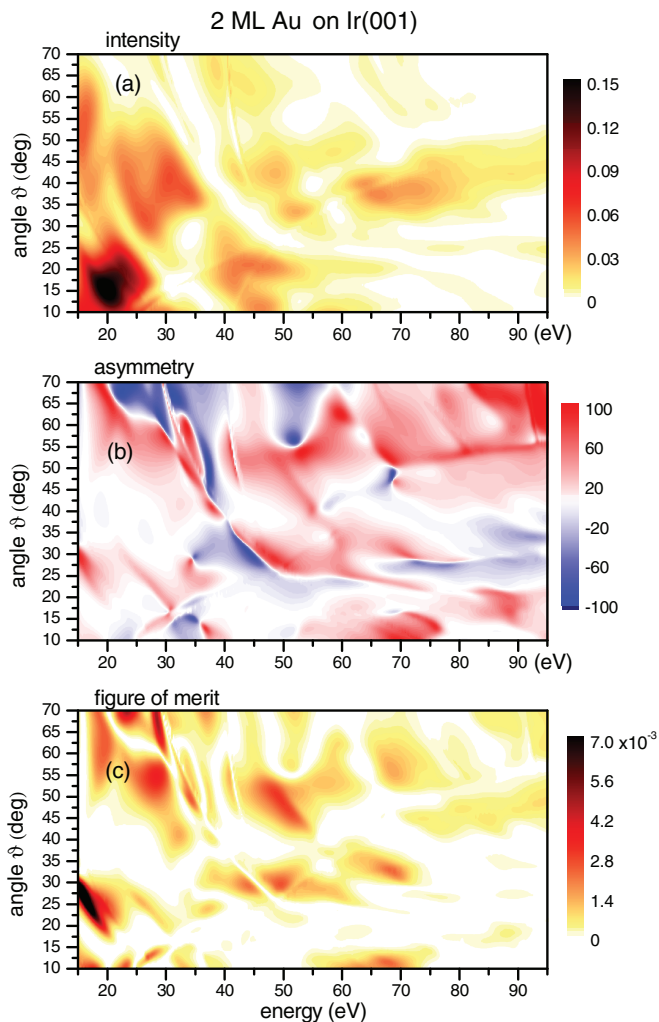


FIG. 3. (Color) Theoretical specular beam intensity, asymmetry, and figure of merit for two pseudomorphic monolayers of Au on Ir(001) as functions of energy and polar angle ϑ for azimuthal angle $\varphi = 0^\circ$.

have been used ever since in a wide variety of LEED surface structure analyses. This kind of measure appears, however, less suitable for asymmetry spectra. Instead, we therefore decided to employ a correlation coefficient, which is customary in statistics for comparing distributions of different variables (cf., e.g., Ref. 38). For adequate comparison, the theoretical results were adapted for the experimental energy and angle resolutions and evaluated on the energy-angular grid of the experimental data. We thus obtained theoretical intensities I_n^{th} and asymmetries A_n^{th} , where the index n runs over the N points of the (E, θ) grid. The corresponding experimental quantities are I_n^{exp} and A_n^{exp} . The averages $\frac{1}{N} \sum_n I_n^{\text{th}}$, etc., are denoted by \bar{I}^{th} , etc. The corresponding standard deviations are $D_I^{\text{th}} := \sqrt{\frac{1}{N} \sum_n (I_n^{\text{th}} - \bar{I}^{\text{th}})^2}$, etc. The correlation coefficient C_{int} between the experimental intensity map and a theoretical one is then defined as $C_{\text{int}} = [\frac{1}{N} \sum_n (I_n^{\text{exp}} - \bar{I}^{\text{exp}})(I_n^{\text{th}} - \bar{I}^{\text{th}})] / (D_I^{\text{exp}} D_I^{\text{th}})$. For the asymmetries, the correlation coefficient C_{asy} is defined analogously. We note that C_{int} and C_{asy} can have values between -1 and 1 . The value 0 means no correlation, whereas values 1 and -1 indicate

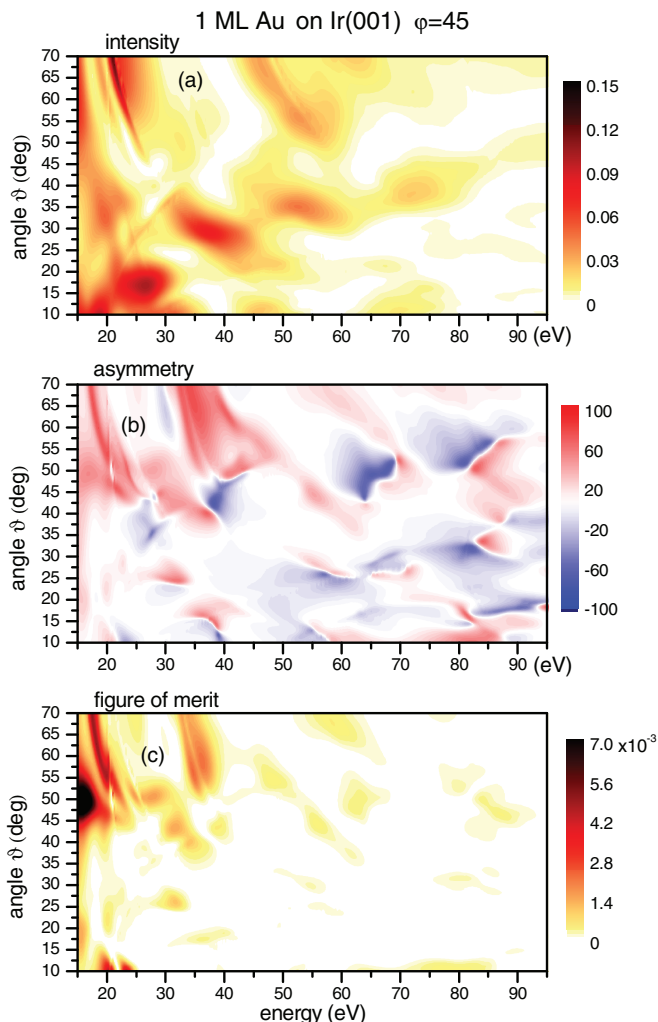


FIG. 4. (Color) Theoretical specular beam intensity, asymmetry and figure of merit for one pseudomorphic monolayer of Au on Ir(001) as functions of energy and polar angle ϑ for azimuthal angle of incidence $\varphi = 45^\circ$ (i.e. surface-parallel momentum component along the [110] direction). The spin orientation axis of the primary beam is the $[-110]$ direction, i.e. in the surface plane and normal to the scattering plane.

perfect correlation and anticorrelation, respectively. We calculated the correlation coefficients between our experimental data on the one hand and each of three theoretical data sets on the other not only for the full (E, ϑ) range shown in Fig. 2, but also for the selected range $15 < E < 60$ eV and $20^\circ < \vartheta < 60^\circ$, which hosts special regions of high figure of merit (cf. Table III). The correlation coefficients, distinguished by the superscripts “full” and “sel,” are shown in Table II. All of them are seen to be largest for 1 ML Au/Ir(001) with azimuth $\varphi = 0^\circ$, distinctly smaller for the 2 ML system with $\varphi = 0^\circ$, and vastly smaller for 1 ML Au/Ir(001) with $\varphi = 45^\circ$. For our experimental azimuth $\varphi = 0^\circ$, 1 ML Au is thus clearly favored over the 2 ML Au. Comparing our experimental landscapes with calculated ones both visually and by means of the quantitative measure “correlation coefficient” thus corroborates our above experimental finding of a pseudomorphic monolayer of Au on Ir(001).

TABLE II. Comparison of correlation coefficients between our experimental landscapes and theoretical ones calculated for 1 and 2 ML Au/Ir(001) for azimuth $\varphi = 0^\circ$ and for 1 ML Au/Ir(001) for azimuth $\varphi = 45^\circ$. The intensity and asymmetry correlation coefficients $C_{\text{int}}^{\text{full}}$ and $C_{\text{asy}}^{\text{full}}$ were obtained from the full (E, ϑ) range shown in Fig. 2, whereas $C_{\text{int}}^{\text{sel}}$ and $C_{\text{asy}}^{\text{sel}}$ result from the selected range $15 < E < 60$ eV and $20^\circ < \vartheta < 60^\circ$, which hosts the special regions of high figure of merit (cf. Table III).

| | $C_{\text{int}}^{\text{full}}$ | $C_{\text{int}}^{\text{sel}}$ | $C_{\text{asy}}^{\text{full}}$ | $C_{\text{asy}}^{\text{sel}}$ |
|---------------------------------|--------------------------------|-------------------------------|--------------------------------|-------------------------------|
| 1 ML Au/Ir $\varphi = 0^\circ$ | 0.885 | 0.831 | 0.531 | 0.621 |
| 2 ML Au/Ir $\varphi = 0^\circ$ | 0.802 | 0.704 | 0.521 | 0.509 |
| 1 ML Au/Ir $\varphi = 45^\circ$ | 0.420 | 0.184 | -0.112 | -0.061 |

Let us now consider in some detail the monolayer maps in Fig. 2, bearing in mind that the shown theoretical results have not been adapted for experimental resolution in order to reveal more features of physical interest. While agreement between experiment and theory in Fig. 2 is generally quite good, there are mainly two types of differences, which we would like to point out and explain. Firstly, the theoretical plots reveal several narrow ridges—most notably in the asymmetry landscape [Fig. 2(e)] from $(E, \vartheta) = (29 \text{ eV}, 70^\circ)$ to $(37 \text{ eV}, 45^\circ)$, from $(40 \text{ eV}, 56^\circ)$ to $(42 \text{ eV}, 50^\circ)$, and from $(42 \text{ eV}, 70^\circ)$ to $(57 \text{ eV}, 40^\circ)$ —which are surface barrier resonances associated with the emergence thresholds of nonspecular LEED beams. These very fine structures are washed out in the experimental plots due to an energy resolution of 0.3 eV and an angular spread of 2° FWHM.

A second type of difference between theory and experiment is the following. In the calculated $A(E, \vartheta)$ plot a negative-asymmetry streak (blue) extends from $(E, \vartheta) = (80 \text{ eV}, 50^\circ)$ to $(95 \text{ eV}, 56^\circ)$ in association with extremely low intensity. This feature is absent in the experimental data. It also vanishes in the theoretical results if we convolute the sharply calculated asymmetry with the experimental angular resolution of 2° FWHM.

In view of potential use for spin polarimetry, we identify in the experimental data several (E, ϑ) regions with a large asymmetry in conjunction with a sizable figure of merit (see Table III). These favorable regions are in good approximation also present in the theoretical (E, ϑ) landscapes.

The availability of different favorable regions allows an optimization of spin polarimeters for different applications. In particular, region R3 with its very high asymmetry appears most suitable for a two-dimensional spin-polarizing mirror in momentum microscopes,⁶ which measure the momentum distribution of monochromatized electrons, e.g., in angle-resolved photoemission. Region R4, which offers a larger

TABLE III. Regions (labeled R1 to R5) of sizable asymmetry and figure of merit in the experimental (E, ϑ) landscapes [in Figs. 2(b) and 2(c)]. As in Fig. 2(b), A in this table is the measured raw asymmetry.

| | R1 | R2 | R3 | R4 | R5 |
|-------------------|----------------|------------|------------|------------|----------------|
| E (eV) | 16.5 ± 1.5 | 28 ± 2 | 39 ± 1 | 47 ± 3 | 49.5 ± 1.5 |
| ϑ (deg) | 25 ± 1 | 56 ± 2 | 45 ± 1 | 53 ± 3 | 30 ± 1 |
| A (%) | 42.8 | 45 | 62 | 33 | 48 |

energy window, recommends itself as a spin-polarizing mirror behind dispersive electron energy analyzers.⁷

The experimental asymmetry, which is shown in Fig. 2(b) and quoted in Table III, is the measured raw asymmetry A_{raw} . The actual asymmetry, i.e., the spin sensitivity of a detector, at any chosen working point (E, ϑ) is $A = A_{\text{raw}}/P_0$, where P_0 is the primary beam polarization given by $P_0 = P_c D_{cp}$, where P_c is the quoted polarization from the photocathode and $D_{cp} = 0.92$ is the degree of circular polarization of the light.³⁹ Our primary beam polarization is thus $P_0 = 0.80 \pm 0.02$. For the high-asymmetry region R3 (cf. Table III) we arrive at an asymmetry (spin sensitivity) of $A = 77.5\%$. To read the actual asymmetry from Fig. 2(b), one has to multiply the numbers at the color bar by 1.25. The actual figure of merit is seen in Fig. 2(c) if one multiplies the numbers at the color bar by $1.25^2 = 1.56$.

Regarding the theoretical landscapes for two monolayers of Au on Ir(001) (Fig. 3), we would like to mention two aspects. Although the intensity, asymmetry, and figure of merit landscapes are quite distinct from those for one monolayer, fine structure ridges are seen to occur, in particular in the asymmetry, along the same (E, ϑ) lines as in the monolayer plots. This is an obvious consequence of the fact that surface barrier resonances are associated with beam emergence thresholds and that the latter are the same for the two structures. Secondly, we look for (E, ϑ) regions, which might be suitable for spin detector purposes. There are such regions close to regions R1, R2, and R4 of the 1 ML system (cf. Table III), but with smaller overall asymmetry and figure of merit. Moreover, region R3, which has the largest asymmetry, does not have a counterpart on the 2 ML system.

Since SPLEED spectra are known to depend sensitively on the azimuthal angle of incidence φ , one may wonder whether the 1 ML Au/Ir(001), which we have explored for $\varphi = 0^\circ$, offers comparable opportunities for $\varphi = 45^\circ$, for which—like for $\varphi = 0^\circ$ —the scattering plane is a mirror plane of the surface system and the asymmetry vector is therefore normal to the scattering plane. In Fig. 4 we show (E, ϑ) landscapes that were calculated for $\varphi = 45^\circ$. Regions of high asymmetry and sizable intensity are seen to exist around $(E, \vartheta) = (16 \text{ eV}, 50^\circ)$ and $(E, \vartheta) = (18 \text{ eV}, 60^\circ)$. Compared to the azimuth $\varphi = 0^\circ$ (cf. Table III), $\varphi = 45^\circ$ altogether is, however, less suitable for spin polarimetry purposes.

VI. CONCLUSION

A pseudomorphic monolayer of Au on Ir(100) was found to be generated easily and reproducibly. Its preparation benefits from different desorption temperatures for Au multilayers and the pseudomorphic Au layer. This makes the Au desorption from a sesquiatomic Au layer (one and a half monolayer) self-limited as long as the desorption temperature of the pseudomorphic layer is not exceeded. Our pseudomorphic monolayer is extraordinarily stable in UHV. We do not know yet for how long, but the useful lifetime certainly is longer than several weeks.

The spacing between the Au layer and the adjacent Ir layer and the spacings between the near-surface Ir layers were determined by *ab initio* calculations in the framework of density functional theory. These calculations also provided

the real part of the quasiparticle potential, which was used in subsequent SPLEED calculations.

For the pseudomorphic monolayer system we measured and calculated two-dimensional maps of spin-asymmetry and reflected intensity with more than 40 000 data points each, covering the energy (E) range of 15 to 95 eV and the angles of incidence (ϑ) from 10° to 70° . In good agreement between experiment and theory, we observed several regions which can be exploited in two-dimensional spin-polarizing mirrors. Regions of high spin asymmetry (up to 77%) with a useful width of ~ 2 eV are to be used in momentum

microscopes, analyzing the spin polarization and momentum distribution of monochromatized electrons, e.g., in angle-resolved photoemission. Other regions with sizable asymmetry around 40% but a larger energy window up to 6 eV are useful as spin-polarizing mirrors behind dispersive electron energy analyzers.

ACKNOWLEDGMENT

We acknowledge the expert technical help by H. Engelhard, D. Hartung, and R. Neumann during this work.

-
- ¹J. H. van der Merwe and F. C. Frank, *Proc. Phys. Soc. A* **62**, 315 (1949).
- ²J. H. Pollard and W. E. Danforth, *J. Appl. Phys.* **39**, 4019 (1968).
- ³J. A. Smerdon, H. R. Sharma, J. Ledieu, and R. McGrath, *J. Phys.: Condens. Matter* **20**, 314005 (2008).
- ⁴S. Kneitz, J. Gemeinhardt, and H. P. Steinrueck, *Surf. Sci.* **440**, 307 (1999).
- ⁵H. J. Elmers, G. Liu, and U. Gradmann, *Phys. Rev. Lett.* **63**, 566 (1989).
- ⁶C. Tusche, M. Ellguth, A. A. Unal, C. T. Chiang, A. Winkelmann, A. Krasnyuk, M. Hahn, G. Schoenhense, and J. Kirschner, *Appl. Phys. Lett.* **99**, 032505 (2011).
- ⁷M. Kolbe, P. Lushchik, B. Petereit, H. J. Elmers, G. Schönense, A. Oelsner, C. Tusche, and J. Kirschner, *Phys. Rev. Lett.* **107**, 207601 (2011).
- ⁸J. Kirschner and R. Feder, *Phys. Rev. Lett.* **42**, 1008 (1979).
- ⁹F. Lohfink, S. Hankemeier, R. Fromter, J. Kirschner, and H. P. Oepen, *Rev. Sci. Instrum.* **83**, 023708 (2012).
- ¹⁰Dehong Yu, C. Math, M. Meier, M. Escher, G. Rangelov, and M. Donath, *Surf. Sci.* **601**, 5803 (2007).
- ¹¹R. Feder, in *Polarized Electrons in Surface Physics*, edited by R. Feder (World Scientific, Singapore, 1985), Chap. 4.
- ¹²Y. F. Liew and G. C. Wang, *Surf. Sci.* **227**, 190 (1990).
- ¹³D. Kutnyakov *et al.*, *Ultramicroscopy* **130**, 63 (2013).
- ¹⁴J. Unguris, D. T. Pierce, and R. J. Celotta, *Rev. Sci. Instrum.* **57**, 1314 (1986).
- ¹⁵R. E. Thomas, *J. Appl. Phys.* **41**, 5330 (1970).
- ¹⁶M. Okada, M. Nakamura, K. Moritani, and T. Kasai, *Surf. Sci.* **523**, 218 (2003).
- ¹⁷S. Ogura, K. Fukutani, M. Matsumoto, T. Okano, M. Okada, and T. Kawamura, *Phys. Rev. B* **73**, 125442 (2006).
- ¹⁸M. Okada, K. Moritani, T. Kasai, W. A. Dino, H. Kasai, S. Ogura, M. Wilde, and K. Fukutani, *Phys. Rev. B* **71**, 033408 (2005).
- ¹⁹M. Okada, S. Ogura, W. A. Dino, M. Wilde, K. Fukutani, and T. Kasai, *Appl. Surf. Sci.* **246**, 68 (2005); *Appl. Catal. A: General* **291**, 55 (2005).
- ²⁰A. V. Ruban, H. L. Skriver, and J. K. Norskov, *Phys. Rev. B* **59**, 15990 (1999).
- ²¹A. Christensen, A. V. Ruban, P. Stoltze, K. W. Jacobsen, H. L. Skriver, J. K. Norskov, and F. Besenbacher, *Phys. Rev. B* **56**, 5822 (1997).
- ²²A. U. Nilekar, A. V. Ruban, and M. Maurikakis, *Surf. Sci.* **603**, 91 (2009).
- ²³J. Kirschner, H. Engelhard, and D. Hartung, *Rev. Sci. Instrum.* **73**, 3853 (2002).
- ²⁴Yu. A. Mamaev, L. G. Gerchikov, Yu. P. Yashin, D. A. Vasiliev, V. V. Kuzmichev, V. M. Ustinov, E. A. Zhukov, V. S. Mikhrin, and A. P. Vasiliev, *Appl. Phys. Lett.* **93**, 081114 (2008).
- ²⁵e beam evaporator EFM-H.
- ²⁶LVR 100, Meadowlark Optics Inc., USA.
- ²⁷Polarimeter PMI VIS, Meadowlark Optics Inc., USA.
- ²⁸Kh. Zakeri, T. R. F. Peixoto, Y. Zhang, J. Prokop, and J. Kirschner, *Surf. Sci.* **604**, L1 (2010).
- ²⁹E. Wimmer, H. Krakauer, M. Weinert, and A. J. Freeman, *Phys. Rev. B* **24**, 864 (1981).
- ³⁰S. H. Vosko, L. Wilk, and M. Nusair, *Can. J. Phys.* **58**, 1200 (1980).
- ³¹For program description see <http://www.flapw.de>
- ³²G. J. P. Abreu, R. Paniago, F. R. Negreiros, E. A. Soares, and H.-D. Pfannes, *Phys. Rev. B* **83**, 165410 (2011).
- ³³J. W. A. Sachtler, M. A. Van Hove, J. P. Biberian, and G. A. Somorjai, *Surf. Sci.* **110**, 19 (1981).
- ³⁴D. S. Wang, A. J. Freeman, and H. Krakauer, *Phys. Rev. B* **29**, 1665 (1984).
- ³⁵M. R. Radeke and E. A. Carter, *Phys. Rev. B* **51**, 4388 (1995).
- ³⁶S. N. Samarin, J. F. Williams, A. D. Sergeant, O. M. Artamonov, H. Gollisch, and R. Feder, *Phys. Rev. B* **76**, 125402 (2007).
- ³⁷J. B. Pendry, *J. Phys. C* **13**, 937 (1980).
- ³⁸I. N. Bronstein, K. A. Semendjajew, and G. Musiol, *Handbook of Mathematics* (Springer, Heidelberg, 2007).
- ³⁹Our photocathode was of the type described in Ref. 24 (Mamaev *et al.*) where a peak value of $P = 90\%$ was reported for optimal fresh preparation, heating only to low temperatures, and high quantum efficiency. Our cathode was 5 years old, stored at room temperature, heated to higher temperature, not optimally activated, and showing a rather low quantum efficiency. Therefore, we cannot expect an intrinsic spin polarization of 90%, but rather assume $P_c = 86\%$.